JACS
JOURNAL OF THE AMERICAN CHEMICAL SOCIETY
Article
Cite This: J. Am. Chem. Soc. 2019, 141, 1067−1073
pubs.acs.org/JACS

Nonresonant Photons Catalyze Photodissociation of Phenol

Kallie I. Hilsabeck,[†,§] Jana L. Meiser,[†,§] Mahima Sneha,[†,§] John A. Harrison,[†,‡] and Richard N. Zare*[,†]

[†]Department of Chemistry, Stanford University, Stanford, California 94305, United States
[‡]Chemistry, Institute of Natural and Mathematical Sciences, Massey University Auckland, Auckland 0632, New Zealand

Supporting Information

ABSTRACT: Phenol represents an ideal polyatomic system for demonstrating photon catalysis because of its large polarizability, well-characterized excited-state potential energy surfaces, and nonadiabatic dissociation dynamics. A nonresonant IR pulse (1064 nm) supplies a strong electric field (4×10^7 V/cm) during the photolysis of isolated phenol (C_6H_5OH) molecules to yield C_6H_5O + H near two known energetic thresholds: the S_1/S_2 conical intersection and the $S_1 - S_0$ origin. H-atom speed distributions show marked changes in the relative contributions of dissociative pathways in both cases, compared to the absence of the nonresonant IR pulse. Results indicate that nonresonant photons lower the activation barrier for some pathways relative to others by dynamically Stark shifting the excited-state potential energy surfaces rather than aligning molecules in the strong electric field. Theoretical calculations offer support for the experimental interpretation.

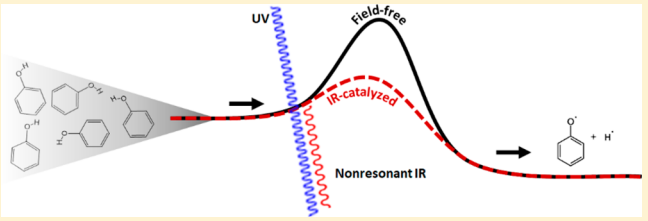

INTRODUCTION

A catalyst is a species that promotes a reaction but is not consumed throughout the course of the reaction. Even for thermodynamically favorable reactions, catalysts are often necessary to achieve appreciable yields because of unfavorable kinetics. Traditional examples of chemical catalysts include enzymes, organometallic complexes, and metal surfaces. By manipulating electric fields around specific bonds or functional groups within a reacting molecule, each of these chemical catalysts provides an alternative reaction pathway with a lower activation energy. The result of this action is to enhance overall reaction rates.

Ostensibly, another type of catalyst could be imagined that instead lowers the original pathway's activation barrier by directly manipulating the energy levels leading to the reaction. Of growing interest in recent years is the idea of photon catalysis: using nonresonant photons to cause reactions to occur that would not take place in their absence.[1−5] The driving force behind this process is the large electric field associated with a focused laser pulse, which for a focal intensity of 10^{12} W/cm^2, is on the order of 10^7 V/cm. For frequencies much greater than the reciprocal of the laser pulse duration, the interaction of the field with a permanent dipole moment averages to zero. Under these conditions, nonresonant radiation interacts with a reacting molecule's polarizability α through its strong electric field.[6] As the system evolves on the potential energy surface from reactants to products, its polarizability and the extent of its interaction with the strong laser field changes. This condition allows for dynamic Stark shifting of the relative energies of the transition state with respect to the reactants and products, thereby lowering the activation barrier for certain pathways. Because the nonresonant light is neither absorbed nor scattered, it acts as a catalyst.

Previously reported observations of photon catalysis are almost exclusively limited to diatomic molecular systems. Stolow and co-workers[1,2] used time-resolved, ultrafast spectroscopy to confirm that application of a strong, nonresonant infrared (IR) field led to substantial changes in the relative contributions of two competing dissociation channels for IBr. More recently, we used nanosecond, near-IR pulses to demonstrate the general effect of photon catalysis on overall product yields in the photodissociation of deuterium iodide (DI).[7] However, the chemical world is not limited to simple diatomic species, and most reactions that are known to require a traditional chemical catalyst involve much larger molecules. To date, Solá, Bañares, and co-workers[3,5] completed the only known study on the effect of strong, nonresonant radiation on a polyatomic molecule. They demonstrated Stark control through production of a light-induced conical intersection in the photolysis of methyl iodide (CH_3I). Still, the utility of photon catalysis on more complex reaction systems requires further investigation.

Molecules containing aromatic rings form the backbone of chromophores in nucleobases and several amino acids.[8,9] As might be expected, their biological significance has stimulated a large body of experimental[8−18] and theoretical[19−26] spectroscopic studies in both gas and condensed phases. In the study presented here, we extend the field of photon catalysis by demonstrating the impact of a strong, nonresonant IR field on the photolysis of the benchmark polyatomic molecule, phenol (C_6H_5OH). Because of its large polarizability, its complex and well-characterized potential energy surface (PES) landscape, and its significance in other areas of science and technology,

Received: October 30, 2018
Published: December 20, 2018

Downloaded via STANFORD UNIV on January 18, 2019 at 18:13:17 (UTC).
See https://pubs.acs.org/sharingguidelines for options on how to legitimately share published articles.

ACS Publications © 2018 American Chemical Society

DOI: 10.1021/jacs.8b11695
J. Am. Chem. Soc. 2019, 141, 1067−1073

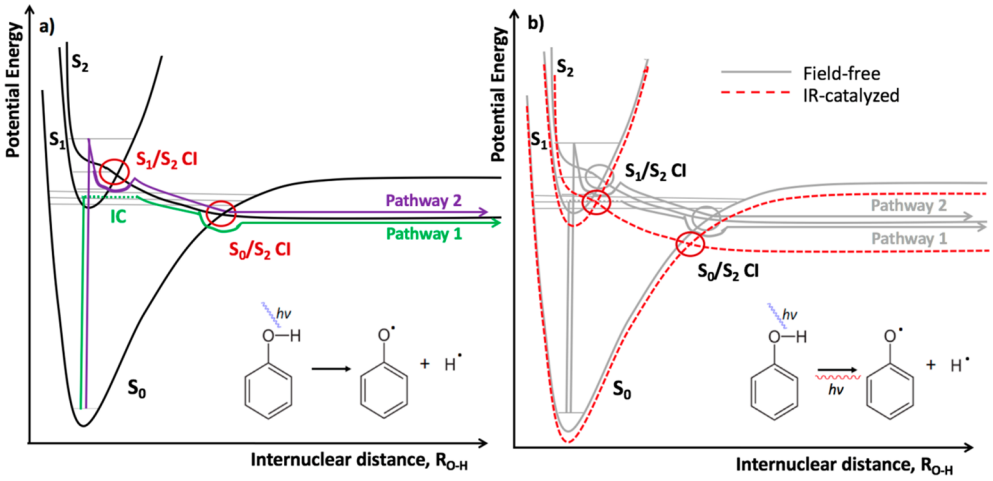

Figure 1. Schematic of (a) field-free potential energy curves of phenol, outlining two major dissociative pathways, and (b) dynamic Stark shift imposed by a nonresonant IR field.

phenol provides an appealing target for the observation of photon catalysis.

Phenol dissociates by breaking its OH bond to yield the phenoxy radical C_6H_5O and an H atom in the wavelength range of approximately 193 to 275.113 nm.[8,9] The latter corresponds to the minimum energy required to excite phenol into the S_1 state. At least two conical intersections (CI) have been reported to be integral to the photodissociation dynamics of phenol at the hydroxyl group.[8−11] These conical intersections occur where the repulsive surface, S_2 ($^1\pi\sigma^*$), becomes degenerate with one of two bound electronic states: the ground state, S_0 ($^1\pi\pi$), and the first excited state, S_1 ($^1\pi\pi^*$) (Figure 1a). Because nonadiabatic dynamics at these conical intersections are expected to be impacted most strongly by the dynamic Stark shift, the nature of phenol's dissociation lends itself well to observation of photon catalysis (Figure 1b).

In a series of pioneering experiments, Ashfold and co-workers[8−11] used H-atom Rydberg tagging to obtain the total kinetic energy release (TKER) of H-atom photofragments produced during ultraviolet (UV) photolysis of phenol. They suggest that the molecule dissociates along two major pathways, one above and one below the S_1/S_2 CI (Figure 1). Experimentally, at $\lambda > 248$ nm, phenol dissociates isotropically through a series of radiationless transitions: internal conversion from S_1 to high vibrational levels within the S_0 manifold and subsequent transfer to the S_2 PES by nonadiabatic coupling at the S_0/S_2 CI (pathway 1, green in Figure 1a). Fragmentation by this mechanism results in the H-atom product speed distribution between 9.5 and 14.5 km/s. In more recent experimental work, Stavros and co-workers concluded that O−H bond fission dynamics below the S_1/S_2 CI in phenol are governed primarily by H-atom tunneling rather than population transfer to acceptor modes in S_0.[27] At $\lambda \leq 248$ nm, a second pathway is also energetically accessible and competes effectively with pathway 1. This pathway, which we refer to as pathway 2 (purple in Figure 1a), involves prompt fragmentation of the O−H bond through direct coupling between the optically excited S_1 PES and the repulsive S_2 PES. This mechanism leads to a distribution of H-atom recoil velocities from 14.5 to 18 km/s. As the excitation energy rises above the S_1/S_2 CI, the H-atom product speed distributions exhibit increasingly dominant features centered around 17 km/s. Collectively, these results imply the existence of a threshold energy near the S_1/S_2 CI above and below which photofragments are formed primarily through different pathways with distinctly different velocities.

In this work, we show the impact of the strong, nonresonant electric field associated with a pulsed IR laser (1064 nm) on two characteristic features of phenol's photodissociation dynamics. First, we access the energetic threshold at the S_1/S_2 CI and change the contribution of each dissociative pathway to the total product yield. Second, we show the impact of nonresonant radiation on the lower dissociation threshold, effectively "turning on" the reaction at wavelengths greater than the field-free $S_1 - S_0$ origin at 275.113 nm. Both observations are evidence of a photon-catalyzed dissociation process.

METHODS

A detailed description of the instrumental setup has been provided in a previous publication.[28] Phenol-h_6 (Sigma-Aldrich) was heated in a reservoir to 50 °C. Argon gas, at a backing pressure of 20 psi, was passed through the reservoir, and the resulting mixture (<1% phenol in argon) was expanded supersonically through a pulsed valve (General Valve, Series 9) into a high vacuum chamber. An additional resistive heating unit was installed at the valve to maintain a constant temperature of 50 °C and to prevent phenol from crystallizing in the valve.[9] The molecular beam was collimated through a 2 mm skimmer and intersected orthogonally by the photolysis (pump) and photoionization (probe) lasers, as well as the IR laser (1064 nm) which supplied the strong electric field. The 1064 nm IR laser pulse is not resonant with any of phenol's rovibrational transitions, which are reported to occur between 3611 cm^{-1} (2769 nm) and 235 cm^{-1} (42 433 nm).[29] Thus, this IR pulse acts as a catalyst. These lasers were overlapped spatially and temporally in the interaction region. A Wiley−McLaren time-of-flight (TOF) mass spectrometer was used in combination with a position-sensitive delay-line detector to obtain the lab-frame speed distributions of the resulting H^+ photofragments. Similar conditions were used for experiments involving phenol-d_6 (Sigma-Aldrich, 99 atom % D), with the subsequent detection of D^+ photofragments.

Phenol-h_6 and phenol-d_6 were photodissociated in the wavelength range between 217 and 275.5 nm. Under each set of conditions, three to five reproducible data sets, averaging over 3000−4000 ions, were collected. The H/D-atom products were ionized using (2 + 1) resonance enhanced multiphoton ionization (REMPI) via the 2s − 1s transition at approximately 243.1 and 243.0 nm, respectively. Under the application of the strong electric field, the REMPI line was red-shifted 10−20 pm to account for the observed Stark shift of the H/D-

DOI: 10.1021/jacs.8b11695
J. Am. Chem. Soc. 2019, 141, 1067−1073

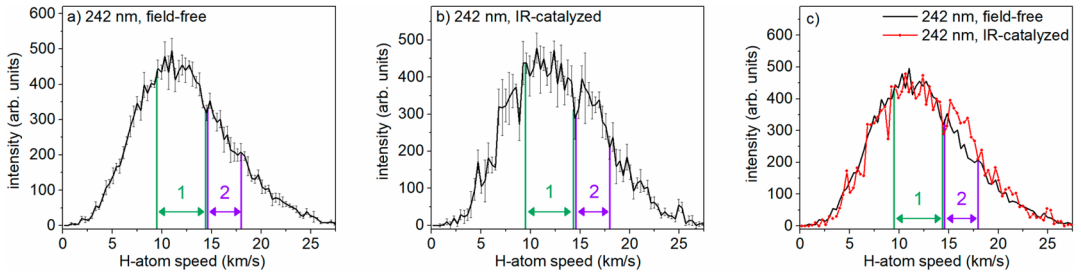

Figure 2. H-atom speed distributions resulting from the photolysis of isolated phenol molecules at 242 nm. Data were collected under (a) field-free and (b) IR-catalyzed conditions. In (c), we overlay the field-free (black) and IR-catalyzed (red) measurements. Error bars represent one standard deviation from the average of 3−5 data sets. Error bars are excluded from (c) for clarity, but differences are significant to one standard deviation.

atom signal. For most experiments, a Doppler-free condition was maintained for the probing step by setting the wavelengths of the two counterpropagating UV lasers such that together they achieved resonance with the 243 nm (2 + 1) REMPI line. The intensity of the laser intended for photolysis was maintained 2−5 times higher at the focus than the intensity of the complementary probe laser to minimize the relative probability of unintentional photodissociation by the probe laser. Minimal contributions to photolysis yield by the probe laser were subtracted as background. Field-free data presented for photolysis of phenol-h_6 at 230 nm was collected via a pump−probe approach, with an optimized 3 ns delay between the photolysis and photoionization lasers.

Some signal events were attributed to nonresonant, multiphoton processes involving the absorption of UV + IR photons. These contributions were subtracted as background. A detailed description of the method of background subtraction is provided in Supplementary Figure 6 and ref 7. Laser powers were chosen to minimize background associated with multiphoton dissociation and ionization processes. Supplementary Figures 7 and 8 present the contributions of pure, isolated signal and accumulated background to the H-atom speed distributions and the signal-to-background ratio dependence on the IR laser fluence. For most experiments, UV laser powers of less than 40 μJ produced sufficient signal. A 1064 nm IR laser pulse focused to an intensity of 2.2×10^{12} W/cm^2 ($\varepsilon_0 = 4.0 \times 10^7$ V/cm) provided the strong, nonresonant electric field. No signal was observed with application of the IR laser alone. This suggests that the field strength used was not high enough to cause nonresonant, multiphoton dissociation and ionization of the molecule.

We generated ultraviolet laser light of appropriate wavelengths for the photolysis and photoionization processes in two ways. We either frequency tripled the output of a dye laser (Lambda Physik, LPD 3000) pumped by the second harmonic of an Nd:YAG^{3+} laser (Spectra Physics, GCR Series) or frequency doubled the output of a dye laser (Lambda Physik, LPD 3000) pumped by the third harmonic of an Nd:YAG^{3+} laser (Quanta-Ray, DCR-3). The strong electric field was supplied by the fundamental of a third Nd:YAG^{3+} laser (Spectra Physics, GCR Series) at 1064 nm. All frequency mixing was achieved using BBO crystals. All three lasers were polarized vertically.

(CASSCF(12,11)/aug-cc-pVDZ) calculations were performed using Gaussian 09.[30,31] Tables S1−S6 provide a detailed description of the calculations.

RESULTS AND DISCUSSION

Effect of Strong, Nonresonant IR Field Near the S_1/S_2 Conical Intersection Energy. Isolated phenol molecules were photodissociated at an excitation wavelength of 242 nm under both field-free and strong, nonresonant field conditions (Figure 2). Speed regions for H atoms produced through photodissociation pathways 1 (green) and 2 (purple) are labeled for clarity. For all experiments presented here, a 1064 nm IR laser pulse focused to an intensity of 2.2×10^{12} W/cm^2 ($\varepsilon_0 = 4.0 \times 10^7$ V/cm) provided the strong, nonresonant electric field. Error bars represent one standard deviation from the mean across 3−5 separate data sets.

As Figure 2 shows, application of a strong electric field to the photodissociation of phenol at 242 nm led to a significant 15% increase in the population of H atoms produced with speeds from 14.5 to 18 km/s (pathway 2) relative to the population of H atoms produced between 9.5 and 14.5 km/s (pathway 1). The observation of an enhancement in pathway 2 qualitatively mirrors the change in previously reported, field-free TKER spectra when the photolysis wavelength is decreased from 244 to 232 nm.[9] From this result, we infer that phenol's interaction with the electric field allowed features in the speed distribution that are not usually present at this low photolysis energy. It should also be noted that the measured speed distributions show significant signals at lower speeds. Low energy H-atom production has previously been attributed to a variety of mechanisms, including multiphoton dissociation processes, that are less well-characterized; therefore, we have chosen to focus primarily on how the relative contributions of pathways 1 and 2 change with the IR field.[10] Small amounts of signal at higher speeds, present in both the field-free and IR-catalyzed distributions, are not explained by previous literature as resulting from pathway 2 and are regarded as artifacts of the method of experimental data collection.

Two possible effects of a strong electric field, alignment of reagent molecules and dynamic Stark shifting of energy levels, could account for the observed change in phenol's dissociation dynamics.[6] Results of a previous study on the photon-catalyzed dissociation of deuterium iodide suggest that the rotational cooling achieved in our molecular beam allows for population of several rotational states for this diatomic molecule and is therefore insufficient to support significant alignment.[7] For larger polyatomic systems, the molecular ensemble is expected to be distributed over an even wider range of rotational states, and state selection of lower-level rotational states would be necessary to achieve detectable alignment.[32,33] Furthermore, neither of the major pathways in the dissociation of phenol are strongly anisotropic. Only pathway 2 has a nonzero anisotropy parameter of $\beta = -0.5$, indicating that the transition has a slight perpendicular character. In the experimental setup employed, both the IR and pump lasers were vertically polarized, with their electric field components oriented parallel to one another; thus, alignment of reagent phenol molecules would be expected to enhance parallel transitions over perpendicular transitions. Therefore, for this system, pathway 2 would be inhibited by alignment. This expectation is opposite the observed change in the H-atom speed distributions as pathway 2, despite its slight perpendicular character, was enhanced in the presence of the strong IR field.

DOI: 10.1021/jacs.8b11695
J. Am. Chem. Soc. 2019, 141, 1067−1073

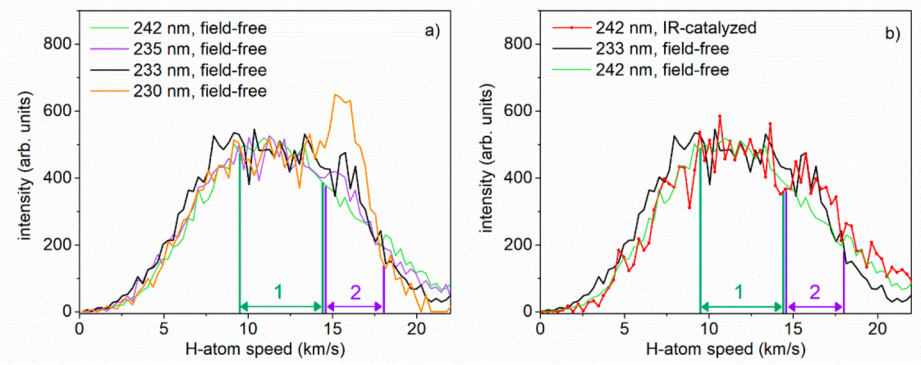

Figure 3. Experimental determination of the Stark shift at the S_1/S_2 CI. (a) Field-free H-atom speed distributions for excitation at 242 nm (light green), 235 nm (purple), 233 nm (black), and 230 nm (orange). (b) Comparison of field-free distribution at 233 nm excitation (black), and IR-catalyzed distribution at 242 nm excitation (red). For reference, the 242 nm field-free distribution is also shown (light green).

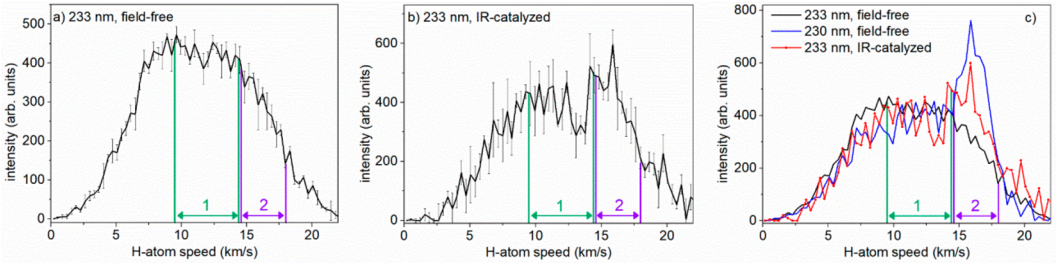

Figure 4. H-atom speed distributions resulting from the photolysis of isolated phenol molecules at 233 nm. Data were collected under (a) field-free and (b) IR-catalyzed conditions. In (c), field-free (black) and IR-catalyzed (red) distributions are overlaid with the field-free distribution at 230 nm (blue). Error bars represent one standard deviation over the average of 3−5 data sets. Error bars are excluded from (c) for clarity, but differences are significant to one standard deviation.

These considerations lead us to conclude that alignment effects are not significant in the present study of photon-catalyzed phenol photodissociation.

Instead, we propose that the strong laser field effectively lowered the activation barrier for prompt dissociation at the S_1/S_2 CI by dynamically Stark shifting the potential energy surfaces and corresponding conical intersections to lower energies. This explanation is consistent with the observed increase in the population of H atoms produced through direct coupling at the S_1/S_2 CI via pathway 2.

We approximated the magnitude of the Stark shift on the S_1/S_2 CI by finding the field-free excitation wavelength that would reproduce the 242 nm, IR-catalyzed H-atom speed distribution. We collected H-atom speed distributions under field-free conditions at several excitation wavelengths below 242 nm. Figure 3a shows the distributions at three of these wavelengths: 235, 233, and 230 nm. In agreement with previous field-free experiments, the yield of H atoms produced with speeds corresponding to pathway 2 increased with an increase in excitation energy.[9,10] The observable change in the higher speed range, between 14.5 and 18 km/s, is modest between 242 and 233 nm, but the field-free distribution at 230 nm clearly shows the extrapolation of this trend. The spike at 15 km/s corresponds to a sharp increase in the probability for dissociation through pathway 2, as molecules are excited above the S_1/S_2 CI that behaves as a barrier to this reaction pathway at higher excitation wavelengths.

A qualitative comparison of the field-free H-atom speed distributions with the 242 nm, IR-catalyzed distribution reveals that, between the four wavelengths presented, the field-free dynamics at 233 nm best approximate the IR-catalyzed dynamics in terms of the relative contributions of pathways 1 and 2 to the overall yield (Figure 3b).

Because of the relatively small changes to the speed distributions within this range of excitation energies, experimental uncertainty precludes a fully quantitative discussion. However, semiquantitative analysis of the H-atom speed distributions supports the qualitative observation: the field-free distributions were integrated in the speed region corresponding to pathway 2 (14.5−18 km/s), and the area in this region of the 242 nm IR-catalyzed distribution is most closely approximated by that of the field-free speed distribution at 233 nm (Supplementary Figure 1). We conclude that the experimental excitation wavelength changes from 242 nm under field-free conditions to effectively 233 nm when the strong IR field is applied. The difference in energy between these two excitation wavelengths is consistent with a lowering of the S_1/S_2 CI by approximately 1600 cm^{-1}.

This result is in qualitative agreement with complete active space self-consistent field (CASSCF(12,11)/aug-cc-pVDZ) calculations which predict that, at the pulsed IR laser intensity used of 2.2×10^{12} W/cm^2 ($\varepsilon_0 = 4.0 \times 10^7$ V/cm), the region of the S_1/S_2 surface crossing corresponding to the 90° out-of-plane H configuration should experience a lowering in energy of 185 cm^{-1} relative to the shifted ground-state energy (Table S6). Although the calculations significantly underestimate the reduction in energy, the differences may be attributed to several factors. First, the calculations assumed an IR field along a single axis which does not describe the isotropic distribution of phenol in the molecular beam. Second, the experimental determination of the Stark shift was semiquantitative, intended to give a mere estimation. Third, as much as any inference can

DOI: 10.1021/jacs.8b11695
J. Am. Chem. Soc. 2019, 141, 1067−1073

be drawn from this limited exploration of the potential surfaces under the influence of an applied field, the prediction that the S_2 state experiences the greatest amount of lowering (ca. 1400 cm^{-1} for S_2; cf. 710 cm^{-1} for S_0) supports our hypothesis that the lowering of the S_1/S_2 CI by the IR field is responsible for the change in the observed dynamics.

To characterize further this threshold effect, we collected H-atom speed distributions at an excitation wavelength of 233 nm, with and without the strong IR field (Figure 4).

The contribution of H atoms produced through pathway 2 was increased by 30% with application of the IR field because of the dynamic Stark effect. The field-free distribution at 230 nm excitation (Figure 4c) clearly illustrates that the speed range enhanced by the IR field correlates with pathway 2. However, the 233 nm IR-catalyzed dynamics do not reproduce the 230 nm field-free dynamics in terms of the relative contributions of the two pathways. On the basis of the estimated Stark shift at 242 nm excitation, we would expect pathway 2 to be enhanced more strongly. As this excess energy is not converted into the kinetic energy of the H-atom photofragment (i.e., the mean speeds for pathway 2 do not change), this observation suggests that it must be contributing to higher internal excitation of the phenoxy radical. Unfortunately, the (2 + 1)-REMPI detection technique has an inherently lower resolution than the H-atom Rydberg tagging method used by Ashfold and co-workers.[8−11] Therefore, we were not able to resolve the vibrational signature of the phenoxy radical in the H-atom speed distributions. Collectively, results presented in Figures 3 and 4 demonstrate photon catalysis of phenol's dissociation through controlled modulation of the relative contributions of two major dissociative pathways to the total product yield.

An isotopic analog of phenol, phenol-d_6, exhibits different dissociation dynamics because of heavier photofragments.[10,11] The nonresonant IR field was applied to the 233 nm dissociation of phenol-d_6 (Supplementary Figure 2).The effect of the strong field was significant to one standard deviation and displayed marked differences from the IR-catalyzed dissociation of phenol-h_6. We present in the Supporting Information more information about the photon-catalyzed photodissociation of phenol-d_6.

Effect of Strong, Nonresonant Electric Field on $S_1 - S_0$ Origin. Our observations near the S_1/S_2 CI support the claim that an intense IR field imposes a dynamic Stark shift on phenol's potential energy surfaces, leading to a change in the overall dynamics of the dissociation process. Returning to the definition of a catalyst as a species that permits reactions that would otherwise not be feasible, these results pose the following question: can we "turn on" the photodissociation reaction under conditions in which it is not normally observed?

As mentioned previously, the minimum energy required to promote ground-state phenol into the S_1 state is reported at an excitation wavelength of 275.113 nm.[9] Below this energy, one-photon dissociation does not occur, and at the origin, dissociation occurs primarily through pathway 1.[8−11] Supplementary Figure 3 presents a representative speed distribution that displays this behavior. To determine if nonresonant IR radiation can lower the $S_1 - S_0$ origin energy and open up pathway 1, i.e., "turn on" the reaction, H-atom speed distributions were measured at an excitation wavelength of 275.5 nm, 51.1 cm^{-1} below the normal dissociation threshold. Negligible photodissociation was attributed to 275.5 nm photons under field-free conditions. Figure 5 reveals the

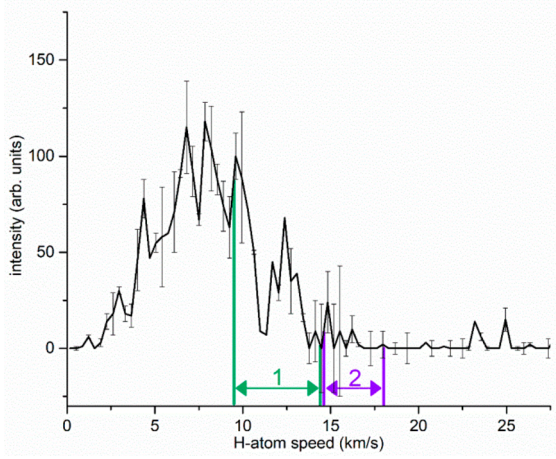

Figure 5. H-atom speed distribution showing the enhancement of phenol photodissociation at 275.5 nm with application of strong, nonresonant IR field. This distribution represents the difference between the field-free and IR-catalyzed speed distributions, i.e., the field-free distribution subtracted from the IR-catalyzed distribution (Supplementary Figure 4). Error bars indicate one standard deviation from the average of three data sets.

enhancement in the photodissociation yield at this photon energy when a strong, nonresonant IR field is applied. The procedure for constructing Figure 5 is presented in Supplementary Figure 4.

Notably, there was a statistically significant enhancement in the otherwise negligible population of H atoms produced at 12.5 km/s. This peak is in the range of speeds corresponding to pathway 1. Furthermore, it is energetically consistent with the most prominent peak, centered at 6000−6500 cm^{-1}, which is equivalent to an H-atom speed range of 12 to 12.5 km/s, in TKER spectra collected at the $S_1 - S_0$ origin.[9] Quantitative agreement provides confidence that the observed peak arises from dissociation at or near the $S_1 - S_0$ origin. The excitation wavelength of 275.5 nm is the lowest photon energy for which we could observe a statistically significant enhancement of pathway 1, allowing for an experimental approximation of the lowering of the $S_1 - S_0$ origin by about 50 cm^{-1}. With this result, we experimentally demonstrated that the reaction can be "turned on" in the presence of the strong IR field: photodissociation via pathway 1 was observed at an excitation wavelength greater than the $S_1 - S_0$ origin.

CASSCF(12,11)/aug-cc-pVDZ calculations predict that, at a pulsed IR laser intensity of 2.2×10^{12} W/cm^2 ($\varepsilon_0 = 4.0 \times 10^7$ V/cm), the electronic ground state and first excited state are downshifted by 710 and 673 cm^{-1}, respectively (Table S6). At this level of theory, the small difference between the electronic-state energies in the presence of a strong field is supportive of the idea that the primary effect of the field on the dissociation dynamics in this region is in shifting the bound surfaces, rather than directly impacting nonadiabatic processes at a conical intersection (cf. CI downshift for the out-of-plane value of 895 cm^{-1}; Table S6).

Experimentally, there was also an enhancement in the population of slower-moving H atoms when the IR field was applied. Figure 5 shows this enhancement at speeds as low as 3 km/s. As stated previously, H atoms produced with these low kinetic energies are conjectured to result from a variety of mechanisms, including multiphoton excitation to superexcited states as well as statistical unimolecular decay of S_0 molecules.

DOI: 10.1021/jacs.8b11695
J. Am. Chem. Soc. 2019, 141, 1067−1073

Although it is difficult to characterize fully how nonresonant radiation may promote these dissociative pathways, an increase in this peak is consistent with results observed at an excitation wavelength at/above the $S_1 - S_0$ origin (Supplementary Figure 3).

Control experiments at 217 nm, the complementary UV wavelength used to achieve the Doppler-free condition, confirmed that 275.5 nm photons contributed negligibly to dissociation under field-free conditions. They also verified that the observed enhancement in Figure 5 did not arise from the impact of the IR field on the 217 nm dynamics. Details are provided in Supplementary Figure 5.

CONCLUSIONS

In this study, a strong, nonresonant IR field was applied to the photolysis of isolated phenol molecules near two known energetic thresholds: the S_1/S_2 conical intersection and the $S_1 - S_0$ origin. In each case, changes in the relative contributions of known dissociative pathways were observed and are concluded to be direct evidence of a photon-catalyzed process via dynamic Stark shifting of excited potential energy surfaces rather than alignment. Simple theoretical calculations give a qualitative agreement with the experiment. Extension of photon catalysis studies to reactions involving other polyatomic molecules, as well as condensed-phase reactions, may build understanding of its potential for applicability beyond fundamental scientific research.

ASSOCIATED CONTENT

Supporting Information

The Supporting Information is available free of charge on the ACS Publications website at DOI: 10.1021/jacs.8b11695.

Semi-quantitative determination of Stark shift; effect of strong, nonresonant electric field on the photodissociation of phenol; H atom speed distribution measured from field-free photolysis of phenol; phenol dissociation; H atom speed distributions from phenol photodissociation; background subtraction method; computational details (PDF)

AUTHOR INFORMATION

Corresponding Author

*rnz@stanford.edu

ORCID

Richard N. Zare: 0000-0001-5266-4253

Author Contributions

§K.I.H, J.L.M., and M.S. contributed equally to this work.

Notes

The authors declare no competing financial interest.

The materials and data reported in this study are available upon request from R.N.Z.

ACKNOWLEDGMENTS

This material is based upon work supported by the National Science Foundation under Grant No. 1464640.

REFERENCES

(1) Sussman, B. J.; Townsend, D.; Ivanov, M. Y.; Stolow, A. Dynamic stark control of photochemical processes. *Science* **2006**, *314* (5797), 278−281.

(2) Stolow, A. Quantum control: May the electric force be with you. *Nat. Chem.* **2014**, *6* (9), 759−760.

(3) Corrales, M.; González-Vázquez, J.; Balerdi, G.; Solá, I.; De Nalda, R.; Bañares, L. Control of ultrafast molecular photodissociation by laser-field-induced potentials. *Nat. Chem.* **2014**, *6* (9), 785−790.

(4) González-Vázquez, J.; Sola, I. R.; Santamaria, J.; Malinovsky, V. S. Vibrationally State-Selective Spin− Orbit Transfer with Strong Nonresonant Pulses. *J. Phys. Chem. A* **2007**, *111* (14), 2670−2678.

(5) Corrales, M. E.; de Nalda, R.; Bañares, L. Strong laser field control of fragment spatial distributions from a photodissociation reaction. *Nat. Commun.* **2017**, *8* (1), 1345.

(6) Friedrich, B.; Herschbach, D. Alignment and trapping of molecules in intense laser fields. *Phys. Rev. Lett.* **1995**, *74* (23), 4623.

(7) Hilsabeck, K. I.; Meiser, J. L.; Sneha, M.; Balakrishnan, N.; Zare, R. N. Photon catalysis of deuterium iodide photodissociation. *Phys. Chem. Chem. Phys.* **2019**, DOI: 10.1039/C8CP06107F.

(8) Ashfold, M.; Cronin, B.; Devine, A.; Dixon, R.; Nix, M. The role of $\pi\sigma^*$ excited states in the photodissociation of heteroaromatic molecules. *Science* **2006**, *312* (5780), 1637−1640.

(9) Ashfold, M. N.; Devine, A. L.; Dixon, R. N.; King, G. A.; Nix, M. G.; Oliver, T. A. Exploring nuclear motion through conical intersections in the UV photodissociation of phenols and thiophenol. *Proc. Natl. Acad. Sci. U. S. A.* **2008**, *105* (35), 12701−12706.

(10) Nix, M. G.; Devine, A. L.; Cronin, B.; Dixon, R. N.; Ashfold, M. N. High resolution photofragment translational spectroscopy studies of the near ultraviolet photolysis of phenol. *J. Chem. Phys.* **2006**, *125* (13), 133318.

(11) King, G. A.; Oliver, T. A.; Nix, M. G.; Ashfold, M. N. High Resolution Photofragment Translational Spectroscopy Studies of the Ultraviolet Photolysis of Phenol-d 5. *J. Phys. Chem. A* **2009**, *113* (28), 7984−7993.

(12) Nix, M.; Devine, A.; Dixon, R.; Ashfold, M. Observation of geometric phase effect induced photodissociation dynamics in phenol. *Chem. Phys. Lett.* **2008**, *463* (4), 305−308.

(13) Tseng, C.-M.; Lee, Y. T.; Ni, C.-K. H Atom Elimination from the $\pi\sigma^*$ State in the Photodissociation of Phenol. *J. Chem. Phys.* **2004**, *121* (6), 2459−2461.

(14) Tseng, C.-M.; Lee, Y. T.; Lin, M.-F.; Ni, C.-K.; Liu, S.-Y.; Lee, Y.-P.; Xu, Z.; Lin, M. Photodissociation dynamics of phenol. *J. Phys. Chem. A* **2007**, *111* (38), 9463−9470.

(15) Solgadi, D.; Jouvet, C.; Tramer, A. Resonance-enhanced multiphoton ionization spectra and ionization thresholds of phenol-(ammonia) n clusters. *J. Phys. Chem.* **1988**, *92* (12), 3313−3315.

(16) Dellonte, S.; Marconi, G. Temperature effects on the photophysical behaviour of phenol and anisole in various solvents. *J. Photochem.* **1985**, *30* (1), 37−46.

(17) Dellonte, S.; Marconi, G.; Monti, S. Isotope effect on the photophysical properties of phenol. *J. Photochem.* **1987**, *39* (1), 33−40.

(18) Iqbal, A.; Pegg, L.-J.; Stavros, V. G. Direct versus indirect H atom elimination from photoexcited phenol molecules. *J. Phys. Chem. A* **2008**, *112* (39), 9531−9534.

(19) Sobolewski, A. L.; Domcke, W. Photoinduced electron and proton transfer in phenol and its clusters with water and ammonia. *J. Phys. Chem. A* **2001**, *105* (40), 9275−9283.

(20) Sobolewski, A.; Domcke, W.; Dedonder-Lardeux, C.; Jouvet, C. Excited-state hydrogen detachment and hydrogen transfer driven by repulsive 1 $\pi\sigma^*$ states: A new paradigm for nonradiative decay in aromatic biomolecules. *Phys. Chem. Chem. Phys.* **2002**, *4* (7), 1093−1100.

(21) Lan, Z.; Domcke, W.; Vallet, V.; Sobolewski, A. L.; Mahapatra, S. Time-dependent quantum wave-packet description of the π 1 σ^* photochemistry of phenol. *J. Chem. Phys.* **2005**, *122* (22), 224315.

(22) Vieuxmaire, O. P.; Lan, Z.; Sobolewski, A. L.; Domcke, W. Ab initio characterization of the conical intersections involved in the photochemistry of phenol. *J. Chem. Phys.* **2008**, *129* (22), 224307.

(23) Xu, X.; Zheng, J.; Yang, K. R.; Truhlar, D. G. Photodissociation dynamics of phenol: Multistate trajectory simulations including tunneling. *J. Am. Chem. Soc.* **2014**, *136* (46), 16378−16386.
(24) Xie, C.; Guo, H. Photodissociation of phenol via nonadiabatic tunneling: Comparison of two ab initio based potential energy surfaces. *Chem. Phys. Lett.* **2017**, *683*, 222−227.
(25) Xie, C.; Ma, J.; Zhu, X.; Yarkony, D. R.; Xie, D.; Guo, H. Nonadiabatic tunneling in photodissociation of phenol. *J. Am. Chem. Soc.* **2016**, *138* (25), 7828−7831.
(26) Bouakline, F. Investigation of geometric phase effects in photodissociation dynamics at a conical intersection. *Chem. Phys.* **2014**, *442*, 31−40.
(27) Roberts, G. M.; Chatterley, A. S.; Young, J. D.; Stavros, V. G. Direct Observation of Hydrogen Tunneling Dynamics in Photoexcited Phenol. *J. Phys. Chem. Lett.* **2012**, *3* (3), 348−352.
(28) Koszinowski, K.; Goldberg, N. T.; Pomerantz, A. E.; Zare, R. N. Construction and calibration of an instrument for three-dimensional ion imaging. *J. Chem. Phys.* **2006**, *125* (13), 133503.
(29) Lampert, H.; Mikenda, W.; Karpfen, A. Molecular Geometries and Vibrational Spectra of Phenol, Benzaldehyde, and Salicylaldehyde: Experimental versus Quantum Chemical Data. *J. Phys. Chem. A* **1997**, *101* (12), 2254−2263.
(30) Dunning, T. H. Gaussian basis sets for use in correlated molecular calculations. I. The atoms boron through neon and hydrogen. *J. Chem. Phys.* **1989**, *90* (2), 1007−1023.
(31) Frisch, M. J.; Trucks, G. W.; Schlegel, H. B.; Scuseria, G. E.; Robb, M. A.; Cheeseman, J. R.; Scalmani, G.; Barone, V.; Mennucci, B.; Petersson, G. A.; Nakatsuji, H.; Caricato, M.; Li, X.; Hratchian, H. P.; Izmaylov, A. F.; Bloino, J.; Zheng, G.; Sonnenberg, J. L.; Hada, M.; Ehara, M.; Toyota, K.; Fukuda, R.; Hasegawa, J.; Ishida, M.; Nakajima, T.; Honda, Y.; Kitao, O.; Nakai, H.; Vreven, T.; Montgomery, J. A., Jr.; Peralta, J. E.; Ogliaro, F.; Bearpark, M.; Heyd, J. J.; Brothers, E.; Kudin, K. N.; Staroverov, V. N.; Kobayashi, R.; Normand, J.; Raghavachari, K.; Rendell, A.; Burant, J. C.; Iyengar, S. S.; Tomasi, J.; Cossi, M.; Rega, N.; Millam, J. M.; Klene, M.; Knox, J. E.; Cross, J. B.; Bakken, V.; Adamo, C.; Jaramillo, J.; Gomperts, R.; Stratmann, R. E.; Yazyev, O.; Austin, A. J.; Cammi, R.; Pomelli, C.; Ochterski, J. W.; Martin, R. L.; Morokuma, K.; Zakrzewski, V. G.; Voth, G. A.; Salvador, P.; Dannenberg, J. J.; Dapprich, S.; Daniels, A. D.; Farkas, Ö.; Foresman, J. B.; Ortiz, J. V.; Cioslowski, J.; Fox, D. J. *Gaussian 09*, Revision D.01; Gaussian, Inc.: Wallingford, CT, 2009.
(32) Holmegaard, L.; Nielsen, J. H.; Nevo, I.; Stapelfeldt, H.; Filsinger, F.; Küpper, J.; Meijer, G. Laser-Induced Alignment and Orientation of Quantum-State-Selected Large Molecules. *Phys. Rev. Lett.* **2009**, *102* (2), No. 023001.
(33) Stapelfeldt, H.; Seideman, T. Colloquium: Aligning molecules with strong laser pulses. *Rev. Mod. Phys.* **2003**, *75* (2), 543−557.

DOI: 10.1021/jacs.8b11695
J. Am. Chem. Soc. 2019, 141, 1067−1073